Sensitivity analysis of optical scatterometry technique for high-aspect ratio trench measurement

Justine Grasland, Delphine Le Cunff, Hoang Lam Pham, Maxime Besacier, Jean-Hervé Tortai

Sensitivity analysis of optical scatterometry technique for high aspect ratio trench measurement

J. Grasland [1,2], D. Le Cunff [1], L.H. Pham[2], M Besacier[2] and JH Tortai [2]

[1] *STMicroelectronics, 850 rue Jean Monnet, 38926 Crolles, France*
[2] *Univ. Grenoble Alpes, CNRS, CEA/LETI-Minatec, Grenoble INP, Institute of Engineering and Management University Grenoble Alpes, LTM, Grenoble F-38054, France*

ABSTRACT

For CMOS image sensors fabrication, deep trenches are commonly incorporated in the device to isolate the individual pixel one another within the pixel matrix. These etched structures typically exhibit a high aspect ratio of 1:20 and controlling such narrow and deep object is a challenge for inline metrology. In a manufacturing environment, the preferred method for trench height measurements remains the optical scatterometry (OCD) technique as being very sensitive and reliable. Still, it requires time and resources for model construction and validation. It appears then that an analysis of its predicted sensitivity could be a valuable pre-step before starting any activity on large periodical objects where OCD sensitivity can reach its limits. In this study, we tested this approach for deep trench structures with CD dimension in the range of 100nm to 1400nm and the depth from 100 nm to 5 µm. The periodicity (pitch) was fixed at CD*2. At first, 3D Mueller scatterometry signatures were modelled selecting spectroscopic ellipsometry acquisition configurations according to industrial most common ones. Thanks to an optimized RCWA (Rigorous Coupled Wave Analysis) code developed in-house, calculation durations were reduced enough to allow massive data generation. By implementing a sensitivity analysis approach that uses Sobol coefficients, the sensitivity of the OCD metrology technique is here evaluated for each CD and depth values. More particulary, it will be illustrated by a CD range of ±10% of 350nm and with the depth of the trench varying from 100nm up to 5µm. As a results, a sensitivity frontier can be estimated at around 3µm, a critical depth value above which OCD in the given configuration is no more sensitive to the metrics determination. Such observation will be further discussed by analysis of convergence evaluation.

Keywords: metrology, trenches, OCD, RCWA, sensitivity analysis, Sobol index, Mueller matrix

1. INTRODUCTION

Currently, imaging products use micrometric size lenses whose role is to focus light onto each photodiode of a sensor pixel. Each pixel is isolated from other ones by trenches. These are called ‘deep trench’ due to their high aspect ratio of 1:20 (cf. Fig. 1). Measurement methods use for the dimensional control of trenches are transmission electron microscopy (TEM) and optical scatterometry also called Optical Critical Dimension (OCD) measurement. This last technique is widely used for measuring the geometric metrics of periodical patterns on surfaces, such as the size and shape of features, by analyzing the scattering of light they reflect [1,2]. It requires physical model, clear knowledge of the material properties, design structures and computation time for model construction and validation [3].

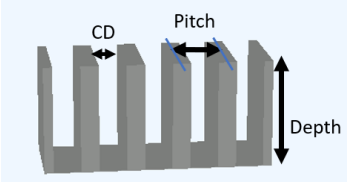

Figure 1: Illustration of periodic trenches

Till recently, clear trend in the industry demand was to reduce the spot size to allow flexibility in measurement structures positioning on the wafer [4]. As an undesired consequence, this can result in a loss of sensitivity for the case of large object measurements simply because only few objects are presented under the beam. Conducting a pre-evaluation step is therefore useful before engaging in new application development and can also provide useful information on optimum measurement configurations. Here, we propose a methodology for evaluating the ability of OCD measurement to measure high aspect ratio elements, applied to deep trenches. We develop a method to evaluate the sensitivity using the Mueller matrix (MM) formalism on periodic trenches. All the study is based on simulated spectra based on an optimized RCWA code developed in-house to simulate the 2D gratings scattering spectra [5].

In this article, the parameters for generating 2D grating scattering spectra will be outlined in the first part as well as a description of the sensitivity analysis method using Sobol coefficients. In the second part, a study on the impact of trench geometry (depth and CD) on spectra will be conducted and results presented using the Mueller matrix formalism. Lastly, the sensitivity of OCD measurements to trench geometry will be evaluated under a scatterometry measurement configuration by comparing the distance between the Mueller matrix response of a chosen trench configuration with response from variable dimensions of trench.

2. METHODOLOGY FOR OCD SPECTRA SENSITIVITY STUDY

2.1 OCD spectra generation

❖ **Spectroscopic ellipsometry**

In this section, we fix OCD measurement conditions for this study with 2D periodic grating. To begin with, spectroscopic ellipsometry allows measurements to be made over a wide range of wavelengths of incident light [6]. The light is composed of two fields: the magnetic field and the electric field. To present the calculations in ellipsometry, we will focus on the electric field. It can be decomposed into a parallel component (p) and a perpendicular component (s) with respect to the plane of incidence. We note the incident electric field:

$$\vec{E}^{\mathrm{i}} = \boldsymbol{E_s^i} + \boldsymbol{E_p^i} \tag{1}$$

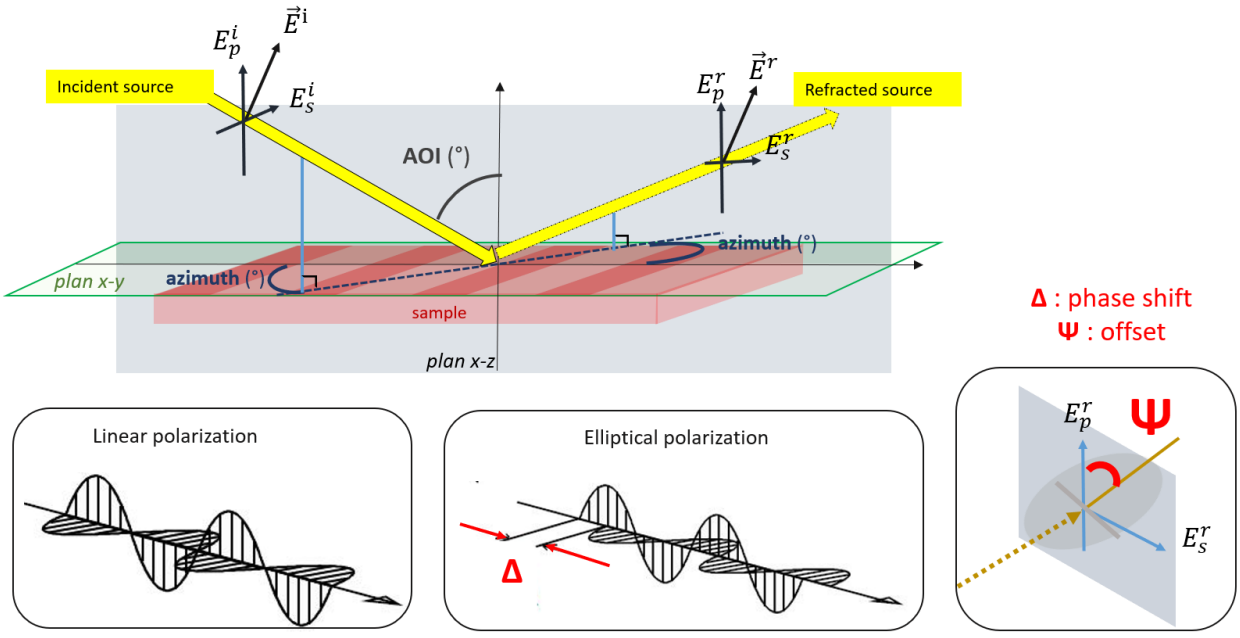

Figure 2: Schematic of an ellipsometry configuration with an azimuthal angle, (x-y plane), AOI angle in x-z plan and an illustration of two polarization states with elements delta and phi.

Fig. 2 illustrates the change in polarization state caused by a sample and characterized by the quantities Ψ and Δ. Psi (Ψ) and delta (Δ) represent respectively the amplitude and phase shift of p- and s-waves. These can be determined from the complex reflectance ρ, which quantifies the polarization change. It is defined as:

$$\boldsymbol{\rho = tan(\psi)e^{i\Delta} = \frac{Rpp}{Rss}} \tag{2}$$

The coefficients Rpp and Rss are respectively used to describe the reflectivity of the light polarized parallel and perpendicular to the plane of incidence r. They are defined by the following formulas:

$$\boldsymbol{Rpp = \frac{E_p^r}{E_p^i}} \qquad \boldsymbol{Rss = \frac{E_s^r}{E_s^i}} \tag{3-4}$$

❖ **Mueller matrix**

Spectroscopic Ellipsometry OCD (SE-OCD) scatterometry configuration gives us Rss and Rpp, but it is possible to extract even more information. Having more points and more coefficients can increase the accuracy and statistical robustness of our study [5–7]. A complete description of the polarization state can be obtained through polarimetry with the use of Mueller matrix (MM-OCD configuration) which takes into consideration the cross-polarization effects of the light. Cross-polarization is a result of the phase difference between the p- and s-polarization components and can be described by the Mueller matrix, while circular polarization is a special case of linear polarization and can be described by the Stokes vector 'S'. The latter, in Eq. 5, is a 4-component vector that describes the polarization state of light in terms of the intensity of light in these four different polarization states.

$$S = \begin{pmatrix} S0 \\ S1 \\ S2 \\ S3 \end{pmatrix} = \begin{pmatrix} E_P E_p^* + E_s E_s^* \\ E_P E_p^* - E_s E_s^* \\ E_P E_s^* + E_s E_p^* \\ i(E_P E_s^* - E_s E_p^*) \end{pmatrix} = \begin{pmatrix} Rpp + Rss \\ Rpp - Rss \\ Rps + Rsp \\ i(Rps - Rsp) \end{pmatrix} \tag{5}$$

The relationship between the Stokes vector and the Mueller matrix can be established by performing a matrix-vector multiplication according to Eq. 6. The Mueller matrix elements can be calculated from the Stokes vector. The Mueller matrix is a 4x4 matrix that describes the change in the polarization state of light after its interaction with the sample. These 16 coefficients represent the amplitude and phase of the reflected light in each of the four polarization states. The coefficients are usually obtained by measuring the intensity of the light in each of the polarization states, and then using these measurements to calculate the matrix elements. In this way, the Mueller matrix can be used to describe the complete polarization state of the light after it interacts with the sample, including cross-polarization effects.

$$\begin{pmatrix} S0 \\ S1 \\ S2 \\ S3 \end{pmatrix}^{out} = \boldsymbol{MM} \begin{pmatrix} S0 \\ S1 \\ S2 \\ S3 \end{pmatrix}^{in} \tag{6}$$

For 2D periodic lines, there is symmetry along both the x- and y-axes. The scattering matrix, by construction, has symmetry between the matrix elements. Those correspond to the same diffraction orders but different polarization states. [5,7] The elements can be normalized according to M11 [8]. Thus nine elements in bold in Eq.8, can describe the Mueller matrix, since: m11= 1,m12= m21, m13= -m31,m14= m41,m32= m23,m42= m24 ,m43= -m34 .

$$\boldsymbol{MM_{initial}} = \begin{bmatrix} M11 & M12 & M13 & M14 \\ M21 & M22 & M23 & M24 \\ M31 & M32 & M33 & M43 \\ M41 & M42 & M43 & M44 \end{bmatrix} \rightarrow \boldsymbol{MM_{final}} = \begin{bmatrix} 1 & \mathbf{m12} & \mathbf{m13} & \mathbf{m14} \\ m21 & \mathbf{m22} & \mathbf{m23} & \mathbf{m24} \\ m31 & m32 & \mathbf{m33} & \mathbf{m34} \\ m41 & m42 & m43 & \mathbf{m44} \end{bmatrix} \tag{7-8}$$

As shown, Mueller measures produce more signals than SE-OCD or SR-OCD and Mueller's spectral sensitivity to structure features variation are stronger in most cases. To study the sensitivity of OCD techniques, we had to choose and enter appropriate parameters to simulate the spectra.

2.2 Configuration for RCWA simulation of periodic trenches spectra

The RCWA method is a computational method that is applied to model the measurement by scatterometry. For 2D grating periods model, the depth of the trenches varies from 100nm up to 4.5µm and pitch in x-direction (Lx) is equal to $2*CD_{ref}$. CD_{ref} varies from 200 nm to 1400 nm. CD equals CD_{ref} ±10%. In y-direction, we consider the line as infinite, so (Ly) as infinite [8]. The lines are composed of silicium with optical index (n,k) dependent of the wavelength. The second material is the air with a refractive index n equals to 1 at standard temperature and pressure. For the angle of incidence (AOI), we chose a value similar with realistic experiment and suppliers advices of 65°. As represented in Table 1, the azimuthal angle corresponding to the plan x-y (cf. Fig. 2), equals 23 °. This value is kept all along the study.

Table 1: parameters chosen for MM-OCD RCWA simulation

Parameters		Values
Angle (°)	AOI	65
	Azimuth	23
Wavelength range [nm]		400 - 2000
Resolution [nm]		1,6
points/spectrum		1000

In RCWA, the diffracted light is decomposed into a finite number of plane waves, each with a different diffraction order. The diffraction order of a plane wave is defined by the values P and Q in x and y direction respectively. These also have an impact on the number of harmonics 'n_harm' that are used to calculate the diffraction of light, the higher the number of harmonics needed to accurately calculate the diffraction of light, the higher the values of P and Q. Their values are chosen according to the multiplication of a factor and the ratio of the period of the structure over the wavelength of the incident light. By choosing the number of diffraction orders to include in the simulation, we can control the level of accuracy of the simulation results and the computation time [5,9,10]. By increasing the factor, the simulation will be more accurate, but it will also be more computationally demanding [11]. For the simulations, the factor is fixed to 11 to have good convergence. Generally, the greater the values of P and Q, the more harmonics "n_harm' are required to accurately calculate the diffraction of light. For the experiment we chose nharm_x = 2*P+1 in x-direction and nharm_y = 1 in y-direction as we are in 2D grating period. Fig. 3 represents one spectrum of silicium trenches obtained with the MM-OCD configuration.

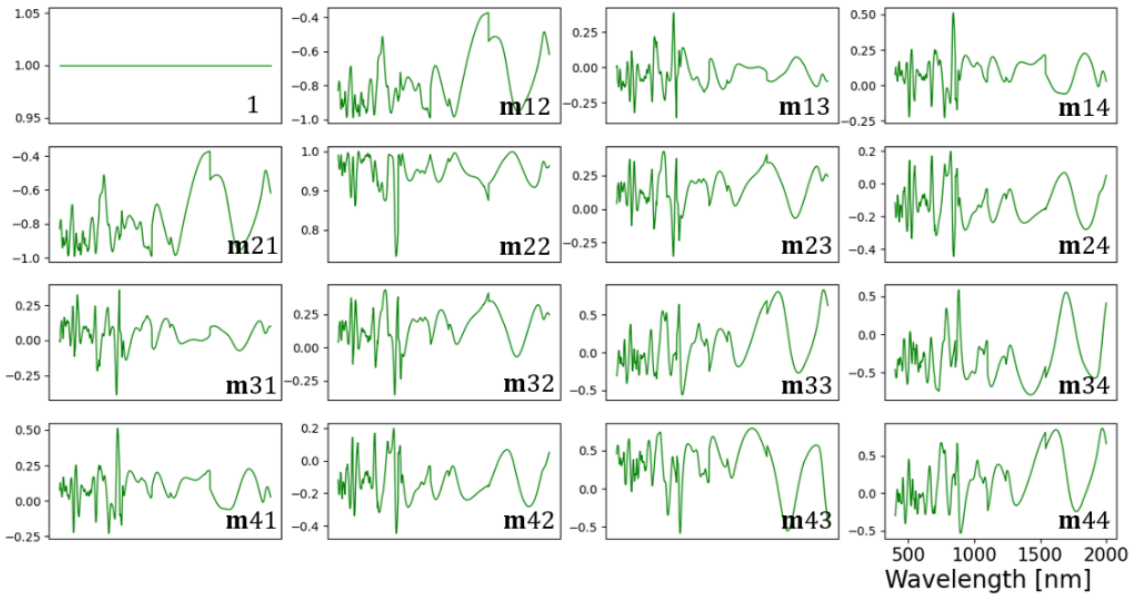

*Figure 3: Simulated Mueller Matrix of trenches of silicon with following dimensions: CD is 350nm, depth is 1000 and Pitch is 350*2=700 nm in MM-OCD configuration described in Table 1.*

These silicium trenches have the following geometry: CD is 350nm, depth is 1000 nm and pitch is CD*2, so 700 nm. Each spectrum of the Mueller matrice is defined between a wavelength range of 400 to 2000 with a number of points of 1000 giving a resolution of spectra equaled to 1.6 nm. Finally, the calculation of the Mueller matrix spectra depending on the geometry of the periodic trenches takes between 1.2 and 2 secondes. Those computation times are fast enough to allow massive data generation for the following sensitivity study.

2.3 Sensitivity approach

The Sobol method based on variance is used to quantitatively evaluate the sensitivity of an output to input parameters [12]. It measures how much the output changes because of changes in the input variables. This method could be applied to many variables such as the bottom and top CD of periodic trenches as well as the depth. For simplification reasons, we consider for this study the top and bottom CD equal to one identical CD. The output is defined here as the 9 Mueller matrix elements, which represent 9 diffraction spectra in relation to the wavelength. To get representative results, the variance of the output is estimated by studying multiple geometries of trenches. We remind that all the outputs/spectra are made by simulation. One other important parameter to be considered in the setting is the choice of sampling, specifically the number of points and their distribution, which affects the average and variance of the output [12,13].

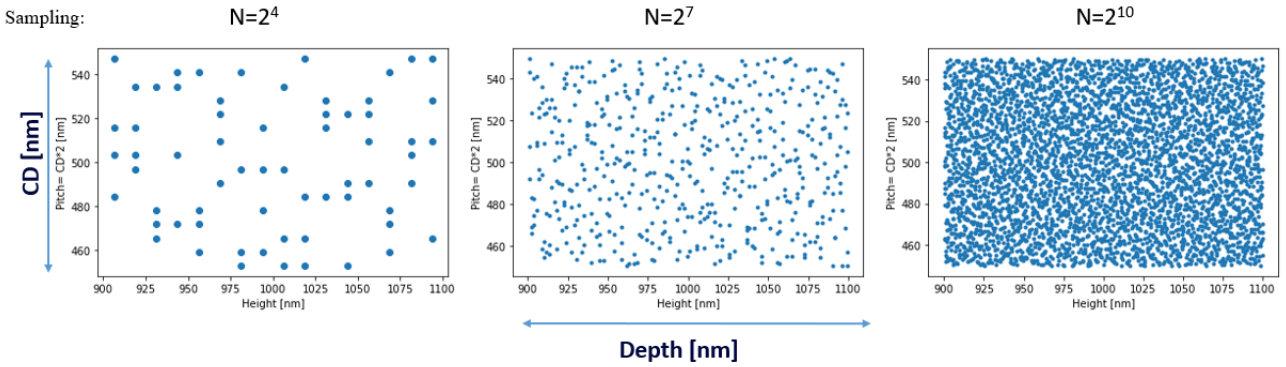

Figure 4: Illustration of the distribution of points by the Sobol sequence, from the smallest to the largest number of points generated

To avoid being influenced by the distribution of points, random sampling can be used. It provides unbiased estimates of the mean and variance of the output. The Sobol' sequence is a low-discrepancy quasi-random sequence that is used to generate uniform samples in the space. Discordance is the maximum absolute difference between a fraction of the area that a square occupies, compared to the number of points it contains. So, the chosen points and geometry are not completely unpredictable, but they are randomly distributed in the given total space (with the minimum optimal number of points). The spread due to discordance can be detected with for example, a low number of points, like $N = 2^4$ (cf. Fig. 4).

To ensure that each input parameter is sufficiently distributed with the same number of points, the Sobol sequence is generated with Latin Hypercube sampling [14,15]. For this, with k number of parameters, the number of samples to generate is $N = 2^k$. The number of input parameters correspond to "D". So, the total number of different geometries is N*(2D+2) or N(D+2), depending on whether the variance is calculated for one parameter (“S1”) or if the variance of the interaction between parameters (“S2”) is included.

The influence of one of the parameters "i", independently of the others, can be calculated with the first order Sobol index "S1". Eq. 9 shows that the closer the coefficient S_i is to 1, the more the global variance of the output varies according to this parameter, and inversely if close to 0.

$$S1 = S_i = \frac{V_i}{V(Y)} = \frac{V\left(E(Y|X_i)\right)}{V(Y)} \tag{9}$$

The model can be considered as a function Y=f(X), where X is a vector of model inputs with 2 variable parameters {Xi, Xj}. The model can be generalized to n variables. With the distribution method used, the inputs are assumed to be

independently and uniformly distributed. Considering the two parameters Xi, Xj then Y can be described as below, with f_0 being a constant and f_i a function of X_i, f_{ij} a function of X_i et X_j.:

$$Y = f_0 + f_i(X_i) + f_j(X_j) + f_{i,j}(X_i, X_j) \quad (10)$$

$$f_0 = E(Y) \quad (11)$$

$$f_i(X_i) = E(Y|X_i) - f_0 \quad (12)$$

$$f_{i,j}(X_i, X_j) = E(Y|X_i, X_j) - f_0 - f_i(X_i) - f_j(X_j) \quad (13)$$

Thus, the variance of the output is influenced by the variable parameters but also by the interaction between them [16], which can be measured with the second order Sobol coefficients "S2" which are defined with the following formula:

$$S2 = S_{i,j} = \frac{V\left(E(Y|X_i,X_j)\right)}{V(Y)} \quad (14)$$

In the same way as for simulation, the first thing to define is the sampling that allows for good assessment repeatability. This quantity N is set based on the confidence interval of the index S1 . A confidence interval of S1 lower than 10% of the value of S1 is chosen and set for each 2D simulation. This gives a value of $N= 2^{10}$ which can be considered as a good compromise between uncertainty and computation time (~1/2 hour for 1024 simulated mueller matrixes using LTM optimized RCWA algorithm on CPU).

3. RESULTS OF MUELLER MATRIX SENSITIVITY ANALYSIS

For each Sobol study, the CD and the depth vary at ± 10% of their value CD_{ref} and $depth_{ref}$ respectively. The pitch influence was not evaluated and was fixed at CD_{ref}*2. In this article, the sensitivity of the OCD metrology technique is reported for given trenches geometry range: depth varying from 100 nm up to 4.5 µm and CD_{ref} varying from 200 nm to 1.4 µm. Each analysis was run using home-made python RCWA program for OCD spectra simulation, SALib API from PyPI library catalog for sampling and for Sobol index generation [17].

3.1 Illustration using m33 matrix element

In this section, two simulations are displayed with a CD of 350 ± 35 [nm] and a fixed pitch value of 700 nm. The depth is variable by 1000 ± 100 and 3000 ± 300 [nm]. Sobol coefficients are calculated for the 9 different spectra of the mueller matrix. Below are plotted the results for the m33 spectrum of the Mueller matrices.

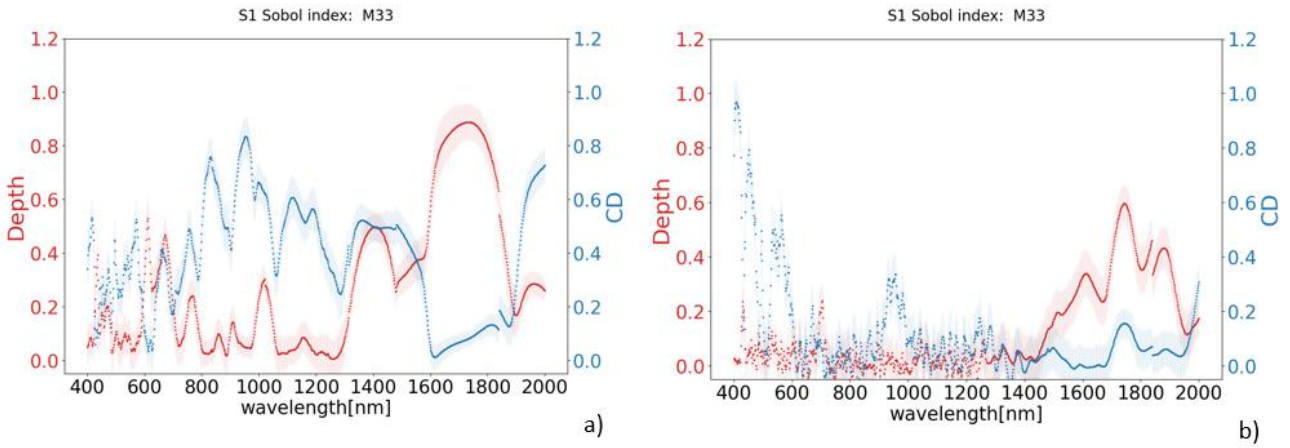

Figure 5: Graphs representing Sobol coefficients for depth and CD as a function of wavelength for spectrum m33. Study on identical CD of 350nm 10%, and two different $depth_{refs}$: a): 1000nm, b): 3000nm

Fig. 5 represents the Sobol coefficients of the depth S1(depth) in red and the one of the CD S1(CD) in blue in function of the wavelength from 400 to 2000nm. Graph a) and b) are respectively the sensitivity analysis of Mueller OCD for trenches with the reference depth of 1µm and 3µm. Graph a) exhibits a general level of S1(CD) around 0.5. For graph b), these peaks vanish and are close to 0. With the increase of $depth_{ref}$ from 1 to 3µm, the values of the Sobol coefficients for the CD in the range of 600 to 1200nm decrease. This means there is a significant global loss of sensitivity of the OCD technique of the CD determination when the depth increase. Graph b) reveals a high sensitivity peak for the CD determination in the wavelength range 400 to 600 nm and a second one less accentuated between 850 and 1000nm. This gives information on the range of wavelength were OCD techniques are the most influenced by the CD. For the graph a), S1(depth) has two major peaks in the 1400 and 1800nm range (respectively close to values of 0.6 and 1). This indicates that the sensitivity to depth seems higher in the IR domain. This is also confirmed by the second graph b) were a major peak appears from 1400nm to 2000nm. Furthermore, it is annotated some points of discontinuities due to the convergence of the spectra that rapidly decrease the variance of S1 index at certain wavelength values. These discontinuities can be observable at different wavelength value depending on the element of the observed matrix. In this case, it is element m33. According to those first result, we expect that OCD sensitivity on metrics determination decreases in most of the wavelength that can be measured when the aspect ratio is increased.

❖ **Local sensitivity results based on m33 element**

To better evaluate the sensitivity to the depth as a function of wavelength, a graph based on m33 data is presented in Fig. 6. The graph is divided into three color areas (Depth x Wavelength) with different sensitive level versus depth for a fixed CD of 350nm ± 3.5nm and a fixed pitch of CD*2. The depth is varied from 100 nm to 5 µm. We suppose that a minimum sensitivity of 15% is sufficient to properly measures the trench depth (green color) while a sensitivity less than 5% is insufficient. Between 5% to 15%, a weak sensitivity is expected. On the graph, we can see that for small depth (<1000nm) almost of the spectra is in a green zone. When the depth of the trenches increases, sensitivity island appears, first for a wavelength range of 400 to 1000nm and a second one from 1200 to 1900nm. The first green zone (meaning that a high sensitivity is expected) quickly becomes orange/red when the depth reaches 2000nm. The second green zone in the Near Infra-Red region shrinks (in the range of wavelength of 1600 to 1800nm) and slowly vanishes when the depth continues to increase. When trenches are deeper than 3000nm, there is no more green zone.

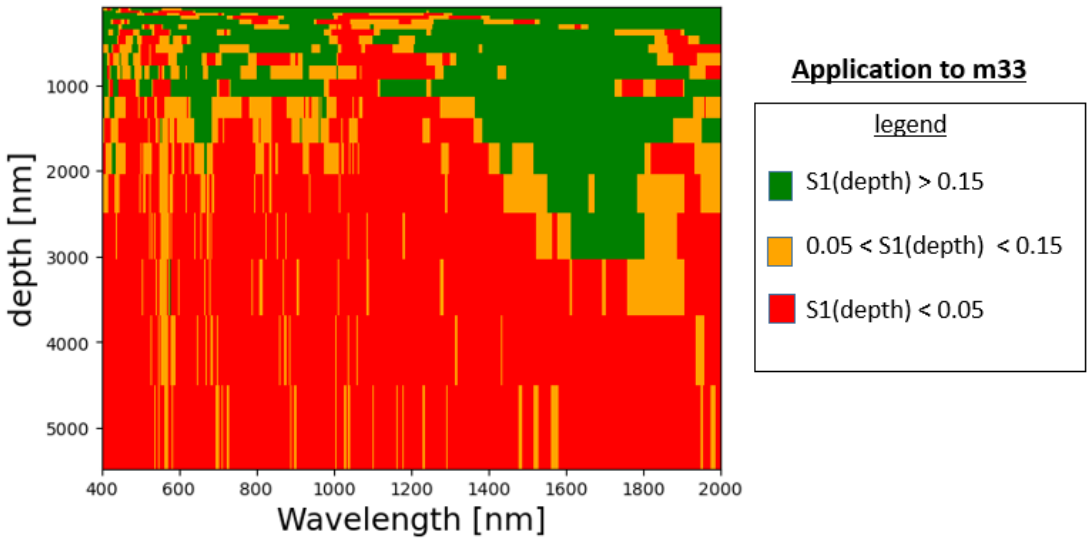

*Figure 6: Graph representing the sensitivity S1(depth) in function of wavelength (nm) and the depth (nm).CD is fixed at 350nm ± 35 nm, the pitch is of CD*2.*

3.2 Illustration with element m14

After exposing the results for Sobol indexes analysis for m33 element, we will briefly present the results for other matrix element to highlight difference in behavior. The Fig. 7 shows the results for the m14 element of the Mueller matrix.

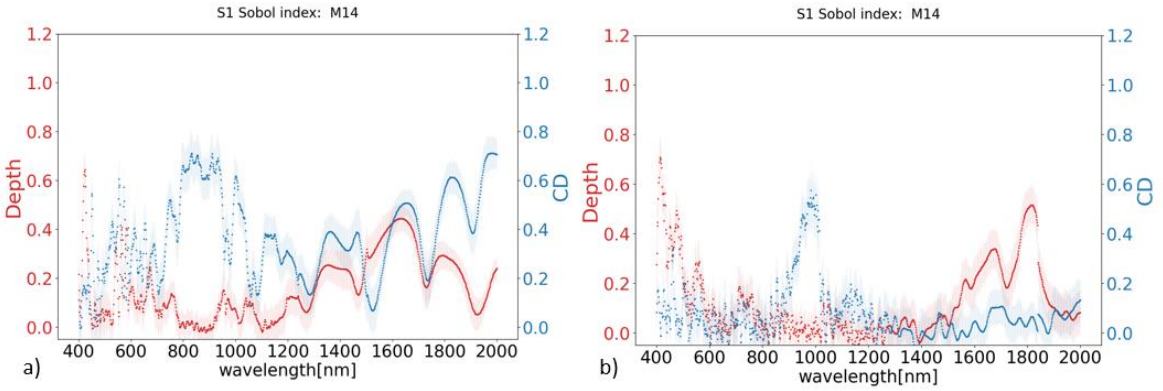

*Figure 7: Graphs representing Sobol coefficients for depth and CD as a function of wavelength for spectrum m14, Study on identical CD of 350nm 10%, and two different depth$_{refs}$: **a): 1000nm, b): 3000nm***

Graph a) and b) correspond respectively to the results of the Depth and CD Sobol coefficients of the reference depth 1µm and 3µm and can be compared with m33 previous studies. We observed somes differences in behavior. For depth sensitivity analysis shown in graph a), we observed now three major peaks for m14 but their correspoding S1 values is smaller compared with m33 behavior. So, we can consider that m14 element has less sensitivity to depth in this wavelength range. But in smaller wavelength, we can see in graph a) Fig. 7, that there is a peak that reach 0.6 at a wavelength close to 400 nm. It seems that there is more sensitivity in the visible domain (especially close to 400 nm) in the case of m14 than m33 according to respectively Fig. 7 and Fig. 5. The graph b) of Fig. 7 confirms this with a peak close to a value of 0.8 at 400nm. This peak is not present in the case of m33. So, the elements m14 and m33 have not the same local sensibility to CD and depth. In fact, regarding their formula, m14 and m33 quantify the change in polarization differently [6]. As Mueller OCD algorithm handles all matrix elements to determine the patterns metrics, only a global sensitivity of the whole Mueller matrix integrating all the measured wavelength can predict the sensitivity of OCD on the determination of high aspect ratio metric of large object.

3.3 Global sensitivity of mueller matrix elements

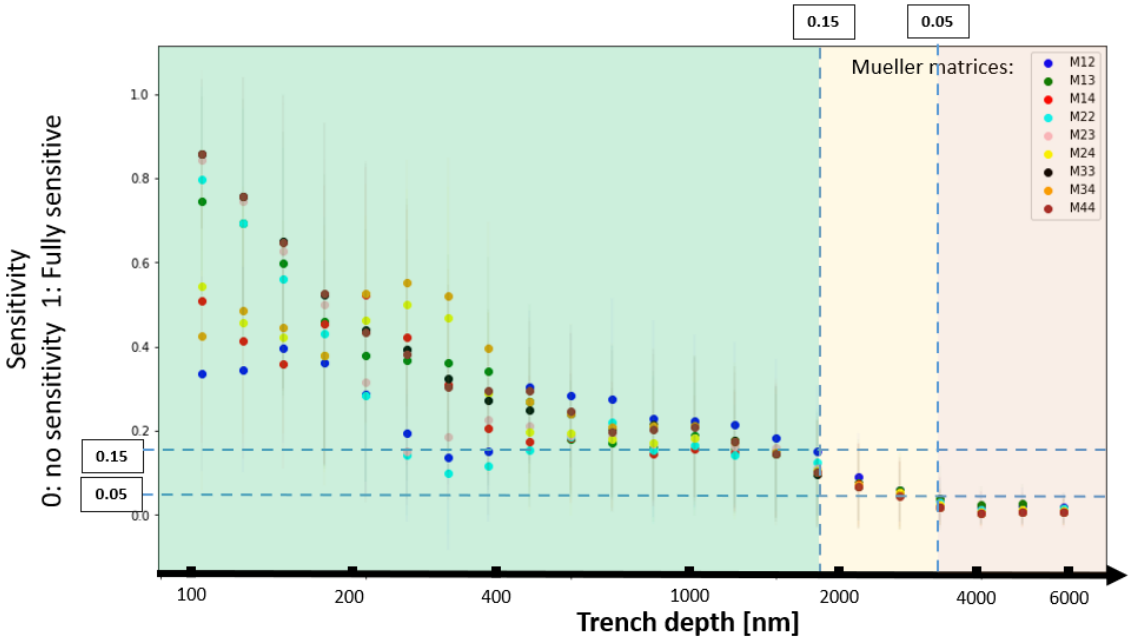

Figure 8: Plot of the average of indexes S1 for each matrix element as a function of trench depth

Fig. 8 represents the mean value of index S1(depth) over the wavelength range of 400 to 2000 nm for 22 values of trenches' depth, varying by 10% of their value, with a CD varying in the vicinity of 350 ± 35 [nm] and a picth of 700 nm. The mean value's calculation for each spectrum is described in Eq. 15, with m_{ij} being the considered element of the Mueller matrix. N is the total number of points (wavelength) on each spectrum.

$$Mean_{mij} = \frac{1}{N}\sum_{k=1}^{n} S1(depth)_{mij}^{k} \tag{15}$$

The coefficients S1(depth) for each matrix are averaged over the wavelength from 400 nm to 2000. It does not take into account the behavior of each element of the matrix at a wavelength but it gives an indication on the behavior and the sensitivity of each matrix to the different trench depths. For example, m34 has a much lower mean sensitivity at 100 nm depth than m22 but over 200 nm it is the opposite. This graph puts in evidence the sensitivity difference to depth variation between the nine matrix elements. Moreover, the curves give an overview of the sensitivity decreasing trend when trenches are deeper and deeper. At an index value of 0.15, all the matrix indexes start to behave the same way and have similar values. This is the critical zone we considered. An asymptotic behavior of S1 (depth) is observed for depth higher than 2µm, whatever the Muller matrix, reaching a value closed to 0.05. With this graph, we have a first representation on the global OCD MM sensitivity and on the threshold value to define sensitive/non senistive frontier for this given sample geometry. According to Fig. 8, OCD simulation with AOI angle of 65° and Azimuth angle of 23° indicates no sensitivity for a depth deeper than 2µm.

4. DISCUSSION

In this last section, we will review the results and discussed about other ways to test for sensitivity evaluation.

4.1 Global grid result of S1(depth)

To better visualize the OCD sensitivity level versus both geometrical parameters which are CD and depth, we created in Fig.9 a 'global grid' schematic of the calculated S1 sensitivity index to depth for m33 element and for the given acquisition configuration (AOI, Azimuth, wavelength, sampling..).

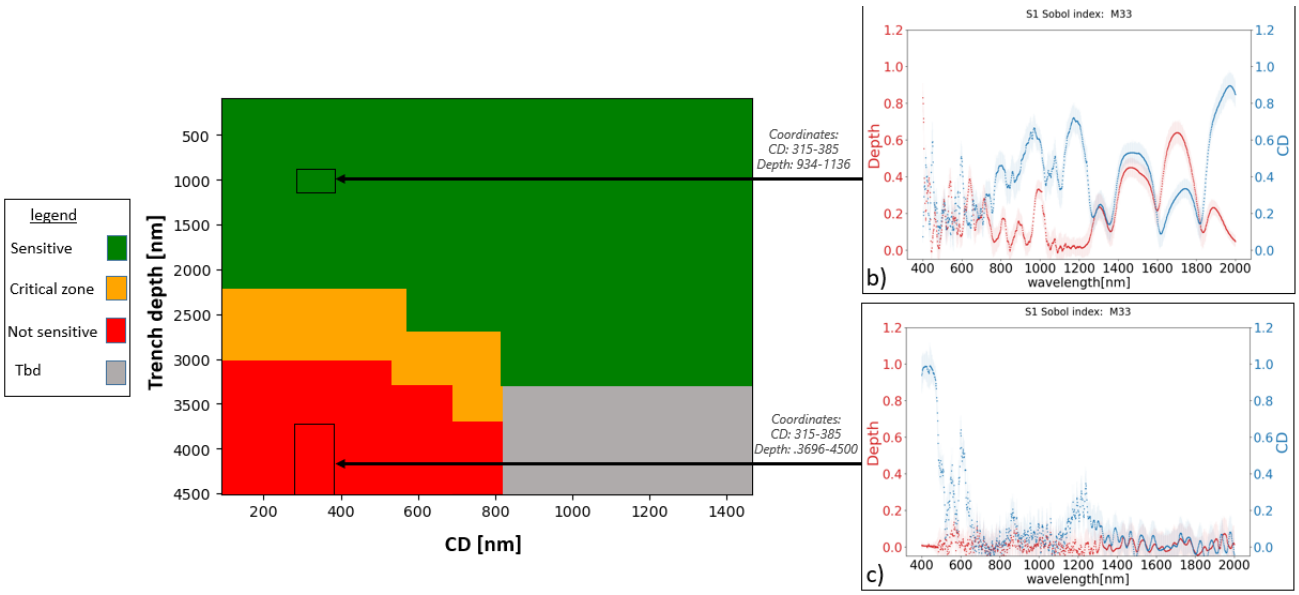

Figure 9: a) Global grid result of scatterometry sensitivity to the depth variable with CD from 100nm to 1.4µm and depth from 200nm to 4.5µm. b), c) Zoom of the results of S1(depth) in function of the wavelength respectively with $depth_{ref}$ around 1000 and around 4000 nm.

The grid, graph a) in Fig. 9 is built with different sampling range of trenches' geometry from which we obtained the Sobol index of S1(depth). For each study with Sobol coefficient, the CD and the depth vary at ± 10% of their value, same as previous studies. The sensitivity is represented with 3 colors. A sensitive zone is defined for which the mean value of the coefficients points S1(depth) is above 0.15 The sensitive zone is in green and not sensitive in red. The orange zone is the critical zone were the mean value is between 0.05 and 0.15. The graph has in x-axis the CD with values from 100 nm to 1400 nm and in y-axis the depth that goes from 200 nm to 4500 nm. Sobol index is sensitive to sampling has explained in paragraph 2.3. Further investigation would be needed to evaluate the influence of the sampling in the critical zone. In fact, in the studied sampling square, some geometries may influence the index value in the wrong way. For the current index calculation, it is a square of 10% of CD_{ref} and $depth_{ref}$ (cf. Fig. 4), but some geometries that are in the same sampling may have different behavior. A higher resolution of 5% is not tested yet in this critical zone but it could be one investigation for smoother and more accurate delimitation.

4.2 Convergence ability versus sensitivity

In parallel with the construction of the global grid, it was decided to conduct a second sensitivity study involving a fitting process between a simulated reference spectrum, with known depth and CD. The objective is to determine if an inverse problem can converge in order to obtain the target geometry. The process consists in monitoring if the global minimum is still well defined when the depth increases for CD values varying from 230nm to 490nm. If the global minimum is centered to the target reference, the minimization algorithm will be capable of matching those of the target. In this way, the sensitivity of the Mueller matrix to the geometry dimensions can be inferred as the spectrum is adjusted to the fit all along the wavelength range. This double check gives us an idea on the geometry that can be fitted with OCD technique. This could help to determine the threshold that says at which S1 index value the OCD technique is not sensitive to one variable. To verify the inverse problem capability, we checked the easiness of convergence (cf. Eq. 16) by calculating the mean square error (MSE) between the signal of a reference geometry dimensions (example: spectrum $m33_{ref}$) with other signals from different geometries ($m33_k$).

$$MSE = \frac{1}{n}\sum_{k=1}^{n}\left(m33_{ref} - \ m33_k\right)^2 \tag{16}$$

n being the number of measured wavelengths.

4.3 Example of convergence ability applied to m33 spectra with different depths.

Fig. 10 (a, c, e and d subscript) is a contour plot that represents how the MSE is distributed around the reference signal in the space of geometry dimensions. Four ($m33_{ref}$) reference signatures were defined to plot Fig 10, the depth being 1000 (a), 2000 (c), 3000 (e) and 4000 nm (g). All the reference trenches CD are set to 350 nm. This graphical representation illustrates the ability to converge to one spectrum. For the CD mesh, the resolution is set to 3nm, from a CD of 230 nm to 490 nm. While for the depth, the simulated spectrum is calculated every 10 nm of depth ref ± 500 nm. The z-axis results are represented using a logarithmic scale of the calculated MSE with a chosen offset coefficient of 10^{-2} to prevent log10(0) divergence.

$$Z = log_{10}(MSE + 10^{-2}) \tag{17}$$

According to the graph a, the global minimum is broad and well centered on the reference values CD_{ref} of 350 nm and $depth_{ref}$ of 1000 nm. It means that a minimization algorithm will easily converge to the reference signal in this space. The more the depth increases, the narrowest the global minimum well is. Moreover, a distortion of the global minimum is observed. At a depth of 4000 nm, graph h) reveals numerous local minima and a strong stretching of the global minimum in the y-direction is appearing (along the depth axis). Higher is the depth, less distinct is the global minimum. To go more into details, we draw a 2D plot of the MSE in function of the CD value from a CD of 300 nm to 400nm. The height is fixed to the reference for the four heights studied. According to graph b, d, f, and h, for a MSE value of 0.075, we have a width that goes from 50nm, 25nm 20 nm to less than 20nm. The global minimum is getting narrower and narrower with the increase height value. It seems that it will be more difficult to get the global minimum with high value of depth trenches. It gives us an indication on the difficulties that could appears to obtain the target values of CD_{ref} and $depth_{ref}$. Less sensitivity could be deduced with this geometry because of higher fitting difficulties, particularly with the depth.

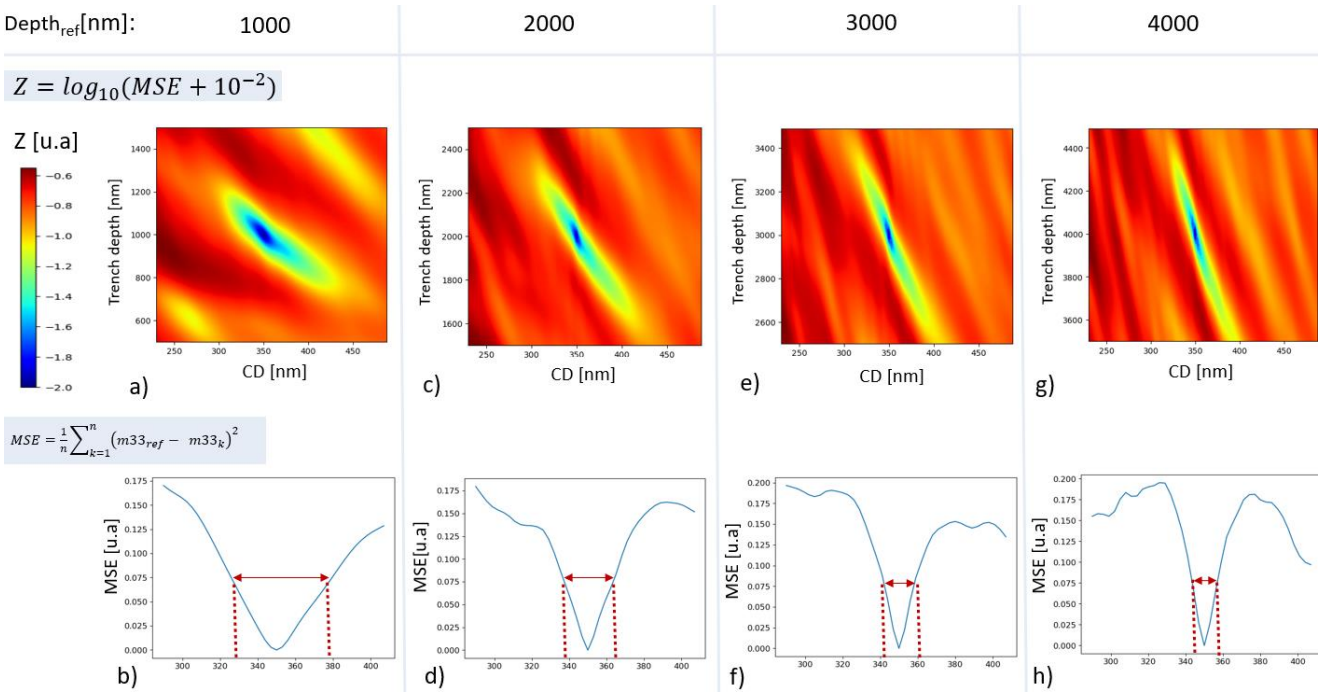

Figure 10: 2D contour plot of CD and depth in function of defined z=f(MSE), graphs a),c),e),g) represent respectively the Plan x,y with CD and depth with z the colorbar. and graphs b), d) f) and h) 2D graphs represent the global and locall minimum in function of CD, with the depth fixed to respectively 1000 nm,2000 nm,3000 nm and 4000 nm.

5. CONCLUSION & PERSPECTIVES

In conclusion, this study showed the sensitivity of MM-OCD simulated spectra to trench measurement for CD geometries ranging from 100 nm to 1.4µm and depth ranging from 200 nm to 6µm. Currently, this study has been conducted using one OCD configuration with an azimuth angle of 23° and an AOI of 65°. For a periodic structure with fixed CD of 350 ± (10% of 350) [nm] and a pitch equals to CD*2, we observe a loss of sensitivity above a trench's depth of 2µm in this MM-OCD measurement configuration. According to the sensitivity study applied to m33 and m14, we observe a loss of sensitivity that is expressed differently according to the wavelength range and to the spectra. A global sensitivity study has been done for the nine Mueller matrix elements. A critical zone has been defined when the Sobol index value of each matrix element seems to be close with the others. For future studies, it may be interesting to examine the influence of sampling on the Sobol coefficients. Some tests can be run with a sampling with higher resolution such as with CD_{ref} and $depth_{ref}$ ± 5%. In addition, a new study with Sobol indexes could be performed using the NI-OCD measurement configuration to compare the results with the MM-OCD configuration. In fact, in the industry, trenches are measured using multiple configurations. They usually complete SE-OCD measurements with normal incidence (NI-OCD) measurements. This latter configuration corresponds to an AOI angle of 0°. It has a normal incident angle which may results in more sensitivity to trench 's depth. Regarding the inverse problem solving, we may deduce a lower sensitivity in some trench shape because of the fitting difficulties but further studies are needed to be able to set a Sobol index threshold value through this double check.

6. AKNOWLEDGEMENTS

We acknowledge the support of European commission, French State and Auvergne-Rhône Alpes region. This work was partly supported by the french Renatech network.

REFERENCES

[1] Diebold AC, editor. Handbook of silicon semiconductor metrology. vol. Chapter 18, New York: Marcel Dekker; 2001, p. 477–514.

[2] Diebold AC, Antonelli A, Keller N. Perspective: Optical measurement of feature dimensions and shapes by scatterometry. APL Materials 2018;6:058201. https://doi.org/10.1063/1.5018310.

[3] Garcia-Caurel E, Ossikovski R, Foldyna M, Pierangelo A, Drévillon B, De Martino A. Advanced Mueller Ellipsometry Instrumentation and Data Analysis. In: Losurdo M, Hingerl K, editors. Ellipsometry at the Nanoscale, Berlin, Heidelberg: Springer Berlin Heidelberg; 2013, p. 31–143. https://doi.org/10.1007/978-3-642-33956-1_2.

[4] Liu S, Du W, Chen X, Jiang H, Zhang C. Mueller matrix imaging ellipsometry for nanostructure metrology. Opt Express 2015;23:17316. https://doi.org/10.1364/OE.23.017316.

[5] Pham H-L, Alcaire T, Soulan S, Le Cunff D, Tortai J-H. Efficient Rigorous Coupled-Wave Analysis Simulation of Mueller Matrix Ellipsometry of Three-Dimensional Multilayer Nanostructures. Nanomaterials 2022;12:3951. https://doi.org/10.3390/nano12223951.

[6] Schweizer T. Handbook of Ellipsometry. Applied Rheology 2005;15:10–1. https://doi.org/10.1515/arh-2005-0022.

[7] Rumpf RC. Electromagnetic and photonic simulation for the beginner: finite-difference frequency-domain in MATLAB, Boston London: Artech House; 2022.

[8] Rumpf RC. IMPROVED FORMULATION OF SCATTERING MATRICES FOR SEMI-ANALYTICAL METHODS THAT IS CONSISTENT WITH CONVENTION. PIER B 2011;35:241–61. https://doi.org/10.2528/PIERB11083107.

[9] Peng S, Morris GM. Efficient implementation of rigorous coupled-wave analysis for surface-relief gratings. J Opt Soc Am A 1995;12:1087. https://doi.org/10.1364/JOSAA.12.001087.

[10] Moharam MG, Gaylord TK, Grann EB, Pommet DA. Formulation for stable and efficient implementation of the rigorous coupled-wave analysis of binary gratings. J Opt Soc Am A 1995;12:1068. https://doi.org/10.1364/JOSAA.12.001068.

[11] Silver R, Germer T, Attota R, Barnes BM, Bunday B, Allgair J, et al. Fundamental limits of optical critical dimension metrology: a simulation study. In: Archie CN, editor., San Jose, CA: 2007, p. 65180U. https://doi.org/10.1117/12.716604.

[12] Campolongo F, Saltelli A, Cariboni J. From screening to quantitative sensitivity analysis. A unified approach. Computer Physics Communications 2011;182:978–88. https://doi.org/10.1016/j.cpc.2010.12.039.

[13] Sobol′ IM. Global sensitivity indices for nonlinear mathematical models and their Monte Carlo estimates. Mathematics and Computers in Simulation 2001;55:271–80. https://doi.org/10.1016/S0378-4754(00)00270-6.

[14] Helton JC, Davis FJ. Latin hypercube sampling and the propagation of uncertainty in analyses of complex systems. Reliability Engineering & System Safety 2003;81:23–69. https://doi.org/10.1016/S0951-8320(03)00058-9.

[15] Lamboni M, Monod H, Makowski D. Multivariate sensitivity analysis to measure global contribution of input factors in dynamic models. Reliability Engineering & System Safety 2011;96:450–9. https://doi.org/10.1016/j.ress.2010.12.002.

[16] Zhang X, Trame M, Lesko L, Schmidt S. Sobol Sensitivity Analysis: A Tool to Guide the Development and Evaluation of Systems Pharmacology Models. CPT Pharmacometrics Syst Pharmacol 2015;4:69–79. https://doi.org/10.1002/psp4.6.

[17] SALib: Tools for global sensitivity analysis. Contains Sobol', Morris, FAST, DGSM, PAWN, HDMR, Moment Independent and fractional factorial methods n.d.